Sonophotocatalytic degradation of aqueous Acid Red 27 and Direct Violet 51 using copper impregnated Al$_2$O$_3$

Fatima Khitab, Muhammad Rasul Jan, Jasmin Shah*

Institute of Chemical Sciences, University of Peshawar, Peshawar 25120, Khyber Pakhtunkhwa, Pakistan, Tel./Fax: +92-91-9216652; emails: jasminshah2001@yahoo.com (J. Shah), fatima_khitab@yahoo.com (F. Khitab), rasuljan@yahoo.com (M.R Jan)

ABSTRACT

Visible-light-driven photocatalyst was prepared by wet impregnation method. The prepared photocatalyst was characterized with different spectroscopic techniques. Copper impregnated alumina (Cu-Al$_2$O$_3$) photocatalyst was used for sonophotocatalytic degradation of two textile dyes, Acid Red 27 (AR-27) and Direct Violet 51 (DV-51). Effect of parameters such as pH, photocatalyst dosage, oxidizing agents, dye concentration, scavengers, photocatalyst's reusability, and catalyst poisoning were investigated. The catalytic degradation of AR-27 increased from 26.8% to 85.1% and DV-51 increased from 23.9% to 84.6% with 8 mmol of hydrogen peroxide. At pH 10, the sonophotocatalytic degradation of AR-27 was 100% in 50 min and DV-51 was 100% in 60 min. It was found that scavengers increased the degradation time and decreased the percent removal of AR-27 from 100% in 50 min to 81.8% in 60 min. Catalyst reusability was checked and used up to five-times, and good results were achieved. Kinetics study was also carried out and found that both of the dyes undergo first order kinetic model. All the experiments revealed that the sonophotocatalytic degradation method in the presence of Cu-Al$_2$O$_3$ is a suitable option for the treatment of textile effluents in the presence of visible light.

Keywords: Impregnated alumina; Textile dyes; Sonophotocatalysis; Oxidizing agents; Scavengers

1. Introduction

Since the last few decades, semiconductors has been established to be one of the most promising methods to solve various environmental problems. Among the various semiconductor photocatalysts applied, TiO$_2$ and ZnO are very common. The photocatalytic activity of TiO$_2$ and ZnO were increased through a doping process using nonmetals, transition metals, rare earth metals, or coupled semiconductors such as ZnO/CuO [1–5]. Modified semiconductor photocatalysts have two types of energy-level systems, which play an important role in charge separation. Coupling of different semiconductors can reduce the band gap, extend the absorbance range to a visible region leading to electron hole pair separation under irradiation, and consequently achieve a higher photocatalytic activity.

Alumina (Al$_2$O$_3$) is a significant material used in nanotechnology due to its high surface area, porous structure, high mechanical and thermal stability, and high catalytic activity. Alumina is considered as a suitable semiconductor alternative to silica [6,7]. Alumina has a wide band gap as a dielectric material, which is a mixture of different crystalline forms of alumina. The reported experimental band gap value for α-Al$_2$O$_3$ is 8.8 eV, for γ-Al$_2$O$_3$ is 7.0–8.7 eV and for am-Al$_2$O$_3$ is 5.1–7.1 eV. It is noteworthy that the band gap value depends on the method of synthesis [8]. A combination transition metal with alumina has many applications in the field of semiconductors and ceramic materials. For improvement of optical and electrical properties, alumina can be doped with transition metals. Due to the partially filled d-orbitals of transition metals, the band

---

* Corresponding author.

gap is extended. Doping of transition metals in alumina change the size of band gap and improve the properties of alumina [9].

Among the dyes, the most commonly used dyes are azo dyes, because they are cost-effective to synthesize than natural dyes. Azo dyes are used in many industries, such as textile, leather, paper, pharmaceutical, paint, and cosmetics. Azo dyes used in textile industries are the major part of all commercial dyes. Azo dyes and their derived products are known to have carcinogenic effect [10]. It is estimated that about 10% of the dye is lost during dyeing processes and are discharged directly into aqueous effluents [11–13]. The disposal of these textile wastewaters poses a major problem for the industry as well as a threat to the environment. The increased public concern about these compounds has promoted the need to develop efficient treatment methods for converting these organic dyes to harmless compounds before its discharge. Different techniques have been developed over the past several decades to find an economic way to treat wastewater of textile dyeing; these methods include flotation, coagulation-flocculation-sedimentation, adsorption, membrane separation processes, biological (aerobic and anaerobic methods), and other technologies. However, most of these treatments are separation techniques that only transfer the pollutants from one phase to another phase. Biological methods present the disadvantages of low biotransformation kinetics, the formation of sludge, and nonresistance to some refractory dyes [14–18]. In addition, some commercial dyes are harmful to some microorganisms. The other common treatment processes, such as adsorption, flocculation, and electrocoagulation, are also not efficient methods because they create environmental problems and only transfer the contamination from one phase to another [19–22]. Recent developments in the field of chemical water treatment have led to an improvement in oxidative degradation processes for organic compounds in applying the combination of photocatalytic and sonolysis methods. They are generally referred as advanced oxidation processes (AOPs) [23,24].

The sonophotocatalytic process of degradation shows advantages due to the synergistic effect between sonolysis and photocatalysis. The combination of sonolysis with photocatalysis called as sonophotocatalysis is considered to be a suitable process for degradation because sonolysis can degrade the hydrophobic products and photocatalysis can degrade the hydrophilic products. In the present work, copper impregnated alumina (Cu-Al$_2$O$_3$) photocatalyst was prepared by wet impregnation method. The photocatalyst was characterized using different techniques. Sonophotocatalytic degradation of AR-27 and DV-51 was used as a model dye for the assessment of Cu-Al$_2$O$_3$ photocatalytic activity under visible light and sonication. To the best of our knowledge, the usage of a sonophotocatalytic process applying Cu-Al$_2$O$_3$ photocatalyst to degrade AR-27 and DV-51 has not been reported previously.

2. Material and Methods

2.1. Chemicals

Analytical grade purity or similar property chemicals were purchased and used without further purification. Alumina (Al$_2$O$_3$) and copper chloride hydrated (CuCl$_2$. 2H$_2$O) were purchased from BDH Laboratory Supplies, Poole, BH151TD, England. Acid Red 27 (molecular formula = C$_{20}$H$_{11}$N$_2$Na$_3$O$_{10}$S$_3$, common name = Amaranth, colour index number = 27905, λ_{max} = 521 nm) and Direct Violet 51 (molecular formula = C$_{32}$H$_{27}$N$_5$Na$_2$O$_8$S$_2$, common name = Violet 2B, colour index number = 27905, λ_{max} = 550 nm) dyes were purchased from Merck Darmstadt, Germany (Table S2). Britton Robinson buffer was used to adjust pH of the dyes solutions.

2.2. Photocatalyst preparation

Photocatalyst was prepared by wet impregnation method reported in our earlier work [25]. The copper metal salt was dissolved in appropriate amount of water to prepare 5%–25% Cu solution for a known weight of Al$_2$O$_3$. Each solution was added dropwise into the slurry of Al$_2$O$_3$ and stirred for 1 h at 900 rpm using 60°C temperature. The catalyst was dried in an oven for 12 h and calcined for 4 h in a furnace at 500°C. The calcined material was crushed and passed by mesh size of ≤150 µm.

2.3. Instrumentation

Ultrasonic bath of 40 KHz (Kum Sung, China) was used as a source of Ultrasonic waves. pH meter (Model-7020 Kent Industrial Measurement Limited Electronic Instrument LTD, Chertsey Survey England) was used for solution pH measurement. UV/vis Spectrophotometer (Model Pharma Spect 1700, Shimadzu, Japan), with matched 1 cm glass cells was used for all spectrophotometric measurements. The solutions were centrifuged on 0–4000 rpm cap: 20 mL × 6 (800–1). All the experiments were conducted under the irradiation of tungsten filament lamp (100 watts). Scanning electron microscope (SEM) JSM5910 (JEOL, Japan) was used for surface morphology analysis of catalysts. The specimens were prepared by coating the samples with a thin layer using double adhesive carbon tape over aluminum stubs for SEM analysis. Energy dispersive X-ray (EDX) was used for the elemental composition of Al$_2$O$_3$ and Cu-Al$_2$O$_3$ catalysts. The surface area was determined by a surface area analyzer (Quanta chrome, Nova Station, A) with nitrogen adsorption–desorption isotherms. The samples were outgassed before the analysis at 100°C for 2 h using high vacuum line in order to remove all the adsorbed moisture or gases from the catalyst surface and pores. The surface area of the sample was calculated using the Brunauer–Emmett–Teller (BET) method [26]. Phase analysis was carried out with an X-ray diffractometer (JEOL model JDX-9C, Japan) at room temperature using monochromatic Cu-Kα radiation (λ = 1.5418Å) at 40 KV and 30 mA in the 2θ range of 10–80° with 1.03° per minute. Band gap was determined by drawing a plot of (Ahv)2 versus hv (ev). Transmission (%) spectrum of 0.05% sample suspension was measured from 200 to 800 nm. Absorbance was measured using A = 2-log%T, after that absorbance of the sample was multiplied by photon energy hv (ev), then plot of (Ahv)2 (direct band gap) as a function of hv (ev) was drawn. Photon wavelength was converted into photon energy by using equation, hv (ev) = 1240/wavelength.

2.4. Photocatalytic study

In a photocatalytic reactor, known volume (100 mL) of dye solution (AR-27 and DV-51) with a desired initial concentration was taken and mixed with optimized weight of photocatalyst (Al_2O_3 and $Cu-Al_2O_3$) in a photoreactor. The photoreactor along with suspension was first placed for 30 min in a dark for adsorption-desorption equilibrium of the dye on the surface of catalysts (Al_2O_3 and $Cu-Al_2O_3$). Then, pH was adjusted to optimum pH 10, and the oxidizing agent (H_2O_2) optimized concentration was added. A wooden box was used to cover the photoreactor setup from stray light. Tungsten filament lamp was used for irradiation of dye solution and the inside was covered with aluminum foil to increase reflection. The photocatalytic degradation process was started by illuminating tungsten filament lamp. With the difference of 10 min, 5 mL was taken from this solution and diluted up to 25 mL (10 μg/mL) with distilled water. The solution was centrifuged at 1500 rpm for 30–45 min to obtain clear solution. Absorbance was measured using UV-vis double beam spectrophotometer at maximum wavelength of AR-27 (λ = 521 nm) and DV-51 (λ = 550 nm). Degradation was calculated using the following equation:

$$\%\text{Degradation} = \left[\frac{C_i - C_f}{C_i}\right] \times 100 \tag{1}$$

where C_i is the initial concentration and C_f is the final concentration of dye solution after irradiation at time t. All the experiments were carried out in triplicate. The degradation conditions were investigated by varying pH, catalyst weight, oxidizing agent, radical scavenger, and initial dye concentration under photocatalytic degradation

2.5. Sonophotocatalytic study

Sonophotocatalytic degradation process was carried out at optimized conditions of photocatalytic degradation. The dye solution with optimum pH, amount of catalyst, and enhancer under tungsten filament lamp (100 W) in an ultrasonic bath (40 kHz ultrasonic waves) was set for sonophotocatalytic degradation. All the sonophotocatalytic experiments were carried out in triplicate. The same procedure was used for calculation of percentage degradation of dyes as used in the photocatalytic degradation process [27–32].

3. Results and discussions

3.1. Catalyst characterization

SEM analysis was performed in order to study the morphology of the catalysts samples prepared with maximum catalytic activity and compared with the support used for impregnation. Fig. 1 shows the morphology of Al_2O_3,
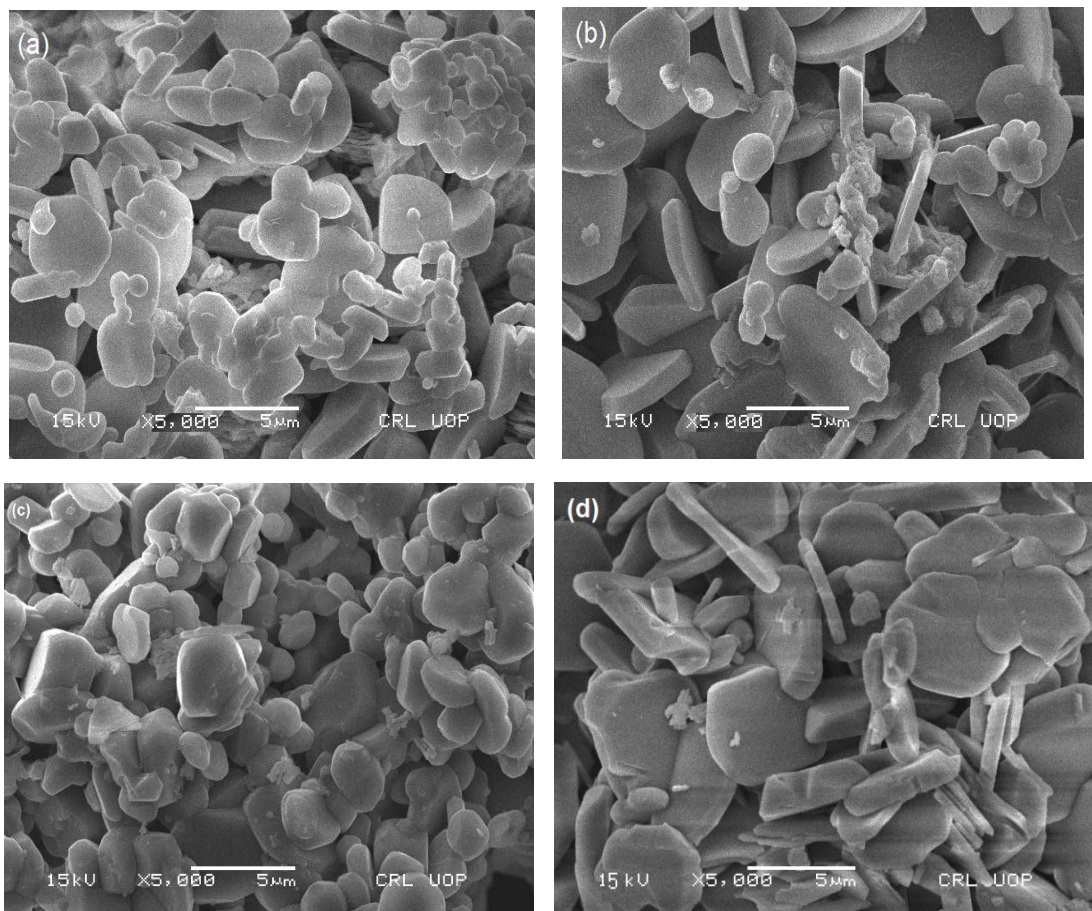

Fig. 1. SEM of (a) Al_2O_3 (b) $Cu-Al_2O_3$ and (c) fifth time reused catalyst (d) fifth time reused catalyst after treatment.

$Cu-Al_2O_3$, fifth time reused catalyst $Cu-Al_2O_3$ and reused catalyst $Cu-Al_2O_3$ after washing. Diverse shapes of small particles are present on the surface of Al_2O_3 after impregnation process of cupper The morphology of fifth time reused and reused after treatment also shows impregnated copper particles.

The EDX spectra for Al_2O_3, 5% Cu impregnated alumina, that is, $Cu-Al_2O_3$ fifth time reused and reused catalyst $Cu-Al_2O_3$ after washing are given in Figs. 2(a)–(d) respectively. The EDX spectra (Fig. 2(b)) show that copper is successfully impregnated on the surface of Al_2O_3 Figs. 2(c) and (d) show that after reusing, the change in concentration of copper is negligible.

Surface area was determined using BET method, and it was found that the surface area of Al_2O_3 was 197.96 m^2g^{-1} and $Cu-Al_2O_3$ was 195.43 m^2g^{-1}. The results revealed that with impregnation there is a small change in the surface area.

Scherer's equation was used for calculation of height, area of the peak, and their respective thickness, and the results are given in Tables S1.1–S1.4 for Al_2O_3, $Cu-Al_2O_3$, fifth time reused $Cu-Al_2O_3$, and reused $Cu-Al_2O_3$ after catalytic treatment. For major reflections, 2θ values range from 11.6° to 78.1°. The last column of the table, where the thicknesses of the crystal lattice calculated by Scherer's

equation, demonstrates that the crystal thickness ranges from 1.55 to 42.56 nm in case of Al_2O_3, 0.72–60.4 nm in case of $Cu-Al_2O_3$ and 1.56–34.1 nm for fifth time reused $Cu-Al_2O_3$ and 2.1–26.8 nm for reused $Cu-Al_2O_3$ after treatment. Particle to particle distance (d) calculated by Bragg's law was in the range of 0.24–1.34 nm for Al_2O_3, 0.24–1.29 nm in case of $Cu-Al_2O_3$ and 0.25 to 1.39 nm for fifth time reused $Cu-Al_2O_3$ and 0.25–1.52 nm for reused $Cu-Al_2O_3$ after treatment.

The XRD for Al_2O_3, $Cu-Al_2O_3$ and fifth time reused $Cu-Al_2O_3$ and after washing is given in Fig. 3, the Al_2O_3 pattern according to ICDD number 11243, 21422, 50712, 100173, 110661, 461131, 490134, 501496, and shows peak at13.2°, 17°, 23°, 25°, 32°, 35°, 37°, 39°, 44°, 52°, 57°, 62°, 67°, 68°, 77°, and 78°, $Cu-Al_2O_3$ shows pattern according to ICCD number 11117, 11142, 11296, 11305, 11307, 20921, 21421, 30892, 40878, 50661, 50667, 80013, and 90440, and Cu shows peak at 43.6°, 50.7°, and 74.4°; fifth time used $Cu-Al_2O_3$ shows pattern at ICDD number 90185, 351401, 11117, 11243, 11296, 50712, 110661, 231009, and 260016; $Cu-Al_2O_3$ after catalytic treatment shows ICDD 90185, 351401, 11117, 11243, 11296, 11304, 21373, 50661, 50712, 110661, 160394, 190010, and 260016. It can be easily observed that 2θ values for major reflections ranges from 13.2° to 78° for Al_2O_3 and $Cu-Al_2O_3$, while 32–75° for fifth time reused and after poisoning

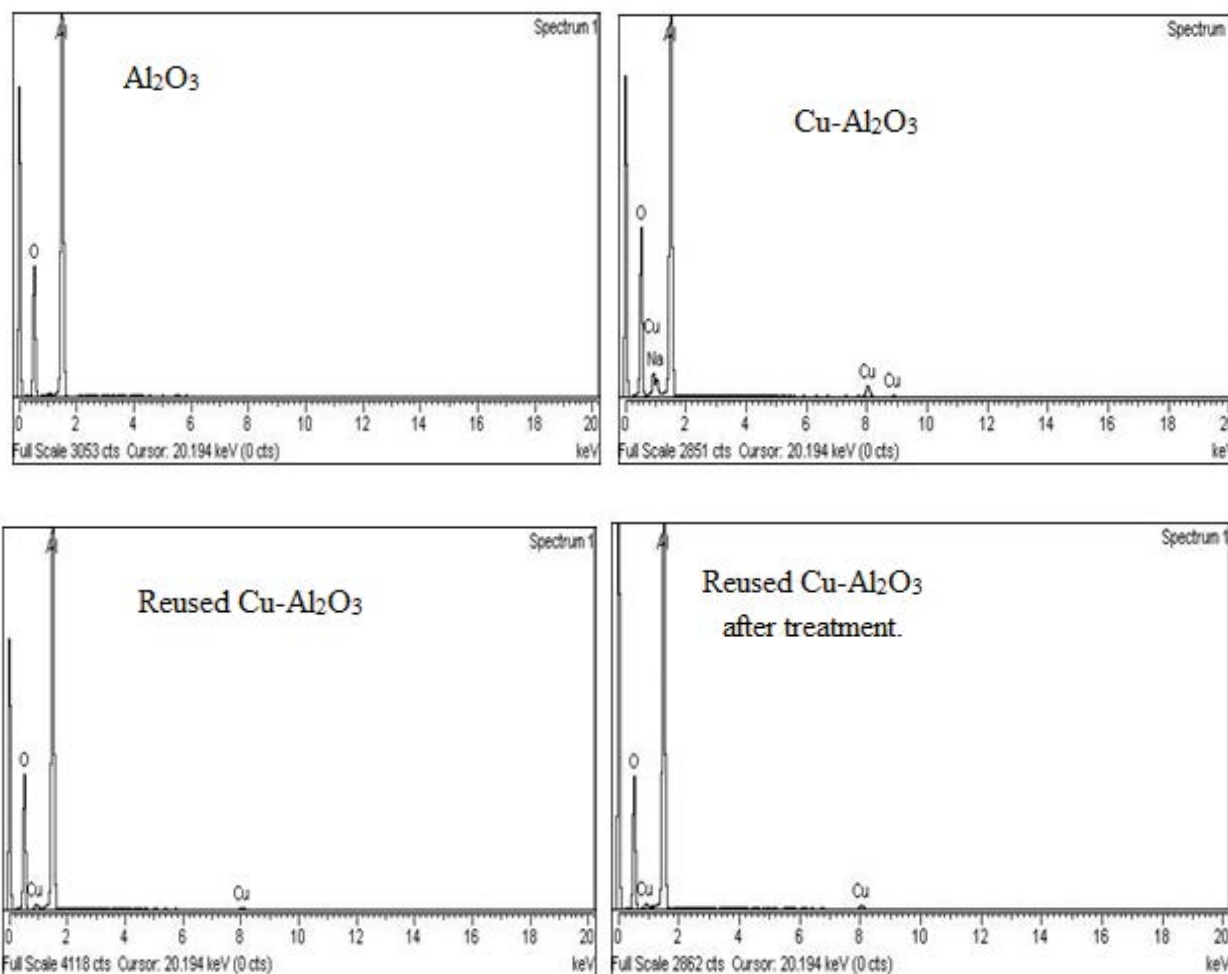Fig. 2. EDX of (a) Al_2O_3 (b) $Cu-Al_2O_3$ and (c) reused $Cu-Al_2O_3$ (d) Reused $Cu-Al_2O_3$ after treatment.
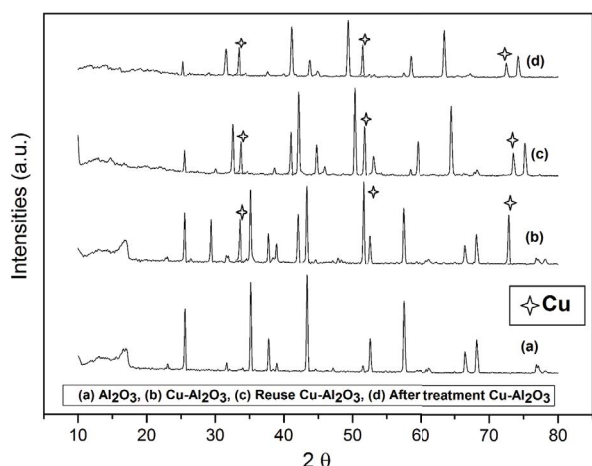
Fig. 3. XRD Pattern of (a) Al_2O_3, (b) $Cu-Al_2O_3$, (c) reused $Cu-Al_2O_3$ and (d) reused $Cu-Al_2O_3$ after treatment.

$Cu-Al_2O_3$. Some residual peaks are also present that might have been absorbed from any residue present in water.

The optical properties of Al_2O_3 and $Cu-Al_2O_3$ were determined through UV-visible spectrophotometric method (Figs. S1(a) and S1(b) in supplementary data). The band gap was determined from the plot of $(Ahv)^2$ versus hv (ev) and the photon energy was calculated from the equation $Eg = 1240/$ wavelength (λ). Copper impregnation shift band gap energy from UV ($Al_2O_3 = 3.6$ ev) to visible region ($Cu-Al_2O_3 = 2.7$ ev). The results revealed that the band gap decreased between the valence band and the conduction band of Al_2O_3 after impregnation with copper.

3.2. Photocatalytic activity

To investigate the shift in band gap of Al_2O_3 after impregnation with copper from UV to visible region, degradation experiments were carried out in the presence of UV and visible irradiation sources (Fig. S2(a)). The results show that degradation of dye was high in the presence of UV light as compared to visible light using Al_2O_3 catalyst. Under the illumination of UV light using $Cu-Al_2O_3$, catalyst decrease in degradation was observed as compared to degradation in the presence of visible light, which confirms that the shift in the band gap is from UV to visible region.

The dyes were degraded under altered conditions like photolysis, photocatalysis, sonolysis, sonocatalysis, and sonophotocatalysis for one hour to study the effect of these processes. AR-27 was adsorbed 6.2% with catalyst and DV-51 adsorbed 17.5%. During the photolysis and sonolysis, no degradation of dyes was observed. However, during photocatalysis and sonocatalysis, AR-27 was degraded up to 12.3% (Fig. S2(b)). While in the case of DV-51, 18.2% photocatalytic degradation was observed and 16.3% sonocatalytic degradation, which was increased to 22.6% sonophotocatalytically (Fig. S2(c)).

3.3. Effect of pH

An important parameter that affects the photocatalytic activity of catalyst and degradation of dye is solution pH.

The effect of pH on the degradation of AR-27 and DV-51 was studied in the range of 2–10. The degradation of AR-27 starts above pH 8 and the maximum degradation (26.8%) was observed at pH 10 (Fig. 4). DV-51 degradation was 21.0% at pH 2 and then decrease in degradation was observed up to pH 8. After pH 8, again degradation increased and 23.90% was achieved at pH 10. The photocatalytic degradation of AR-27 dye was higher in alkaline pH than in acidic. At acidic pH, the decrease in degradation of AR-27 may be due to agglomeration of $Cu-Al_2O_3$ catalyst at acidic pH, which results in decrease in surface area and in turn decreases the photon absorption. In the degradation process of azo dyes, the azo linkage (–N=N–) is exposed to an electrophile attack by OH· radical but in acidic pH, the H^+ ions interact with azo linkage and decrease the electron density at azo group. Therefore, the decrease in reactivity of OH· radicals through the electrophilic attack results in the decrease in degradation of azo dye. Consequently, the increase in degradation of AR-27 at higher pH may be due to an increase in the formation OH· radicals. In alkaline solution, the OH· radicals are also formed from hydroxide ions.

$$OH^- + hv / us \rightarrow OH^\bullet \qquad (2)$$

Maximum degradation of DV-51 was observed at pH 2 and pH 10. The results at pH 10 were more reliable and satisfactory. Because the time required for DV-51 degradation was longer at pH 2 than pH 10. At lower pH (pH 2), the increased decolorization is due to the increased adsorption of DV-51 through electrostatic interaction between positively charged surface of photocatalyst and negatively charged DV-51 dye. The electrostatic attraction decreased with the increase in pH and resulted in the decrease in decolorization of DV-51. At higher pH (pH-10), the increase in concentration of hydroxyl ions leads to the increase in concentration of OH· radicals and resulted in the increased degradation of DV-51. Similar trend was observed and reported by Mahajan et al. in their study on the sonocatalytic degradation of basic red-2 in aqueous solution [33].

3.4. Effect of photocatalyst loading

Photocatalyst amount was optimized in the range of 0.01–0.30 g/L to check the effect on the degradation process of dyes. It was observed that with a very small quantity
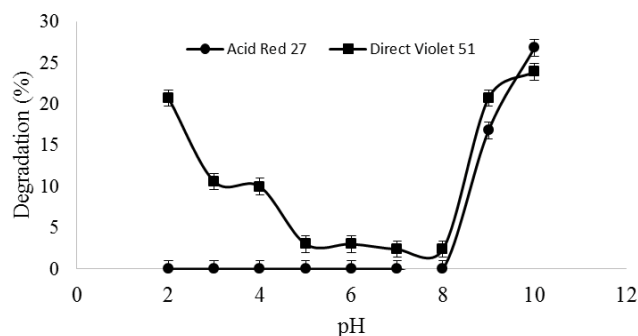

Fig. 4. Effect of pH on the degradation of AR-27 and DV-51. Conditions: Robinson Briton buffer, 0.1 g $Cu-Al_2O_3$, tungsten filament lamp (100W).

(0.02 g/L) of catalyst Cu-Al$_2$O$_3$, about 87.3% degradation of AR-27 found. In case of DV-51, the addition of catalyst speeds up the reaction up to 0.04 g/L with 89.7% degradation. Further increase in the amount of catalyst leads to the decrease in degradation of AR-27 and DV-51 dyes (Fig. 5). The decrease in degradation of dyes may be because of the decrease in the active sites of the catalyst for generation of OH· radicals due to aggregation of catalyst particles in the solution. It may be due to a large amount of photocatalyst that results in the scattering of light and in turn decreases the degradation rate. Furthermore, it also decreases the transparency of solution, which prevents the penetration of radiation down into solution.

3.5. Effect of enhancers

On the photocatalytic degradation of AR-27 and DV-51, the effect of different enhancers, such as hydrogen peroxide, sodium perchlorate, and potassium peroxydisulphate oxidizing agents were investigated. These oxidizing agents generate free radicals, which convert the dyes and convert them into CO$_2$ and H$_2$O through degradation process. Reactions of the hydroxyl radicals are given in the following equations and the mechanism was also reported by many researchers [34,35].
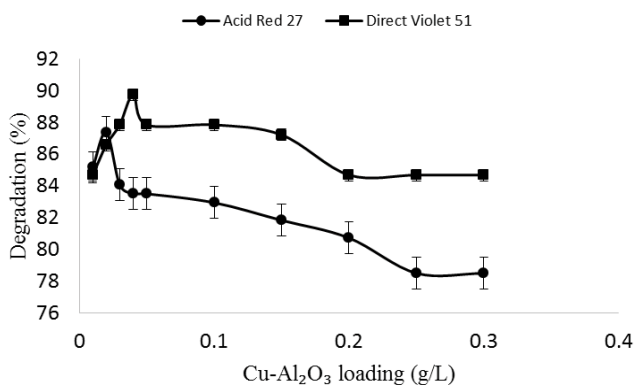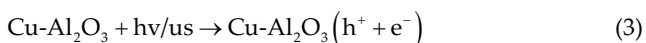
$$Cu\text{-}Al_2O_3 + hv/us \rightarrow Cu\text{-}Al_2O_3\left(h^+ + e^-\right) \tag{3}$$

$$H_2O_2 + hv/us \rightarrow OH^\bullet + H^+ \tag{4}$$

$$H_2O + hv/us \rightarrow OH^- + H^+ \tag{5}$$

$$OH^- + h^+ \rightarrow OH^\bullet \tag{6}$$

$$n OH^\bullet + C_{20}H_{11}N_2Na_3O_{10}S_3 \rightarrow 20CO_2 + 3SO_4^{2-} + 2NO_3^- + nH_2O \tag{7}$$

$$O_2 + e^- \rightarrow {}^\bullet O_2 \tag{8}$$

$$n{}^\bullet O_2 + C_{20}H_{11}N_2Na_3O_{10}S_3 \rightarrow 20CO_2 + 3SO_4^{2-} + 2NO_3^- + nH_2O \tag{9}$$

For AR-27, the results are given in Fig. 6(a) and for DV-51 in Fig. 6(b). The enhancer study was carried out in the range from 3 to 8 mmol, at optimized conditions. With 8 mmol of hydrogen peroxide, sodium perchlorate, and potassium peroxydisulphate, the catalytic degradation of AR-27 increased from 26.8% to 85.1%, 29.6%, and 47.3% respectively and increased from 23.9% to 84.6%, 47.3% and 40.3% degradation of DV-51 with 8 mmol of all three oxidizing agents.

At 8 mmol of H$_2$O$_2$ more OH$^\bullet$ radicals are generated which increases the rate of degradation. Above 8 mmol OH$^\bullet$ radicals react with H$_2$O$_2$ and produces HO$_2^\bullet$. As HO$_2^\bullet$ radicals are not as much reactive like OH$^\bullet$ and enhancement of these radicals contribute to retard the degradation at higher concentration [36].

$$H_2O_2 + OH^\bullet \rightarrow HO_2^\bullet + H_2O \tag{10}$$

The rate of OH· radical formation increases in the case of hydrogen peroxide by the synergistic effect of photon (hυ) and ultrasonic waves (us), which promotes the dye degradation.

The effect of sodium perchlorate on the dye degradation is because of capturing of the electron, which generated on the photocatalyst conduction band (Eq. (11)) [37].
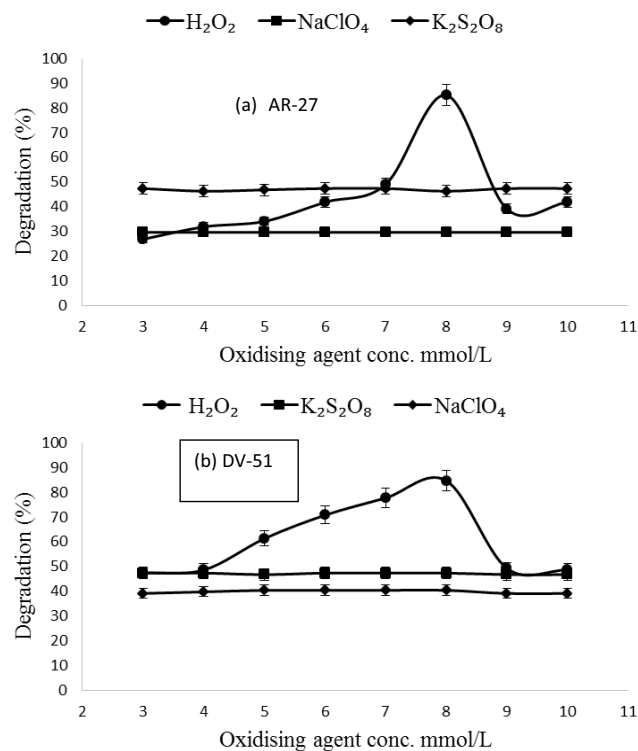
$$ClO_4^- + 8e^- + 8H^+ \rightarrow Cl^- + 4H_2O \tag{11}$$

Fig. 5. Effect of catalyst amount on the degradation of AR-27 and DV-51. Conditions: pH 10, 0.02g Cu-Al$_2$O$_3$ for AR-27, 0.04g for DV-51, tungsten filament lamp (100W).
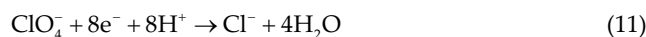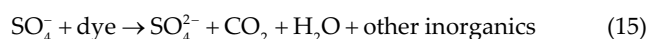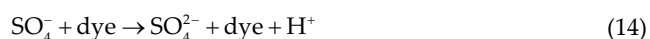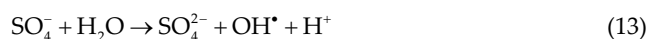
Fig. 6. Effect of oxidizing agent on degradation of (a) AR-27 and (b) DV-51. Conditions: pH 10, 0.02g Cu-Al$_2$O$_3$, 8 mmol of H$_2$O$_2$ for AR-27, 0.04g and 8 mmol of H$_2$O$_2$ for DV-51, tungsten filament lamp (100W).

The effect of potassium peroxydisulphate on dye degradation as an enhancing agent is also increased due to the formation of sulphate radicals, and those sulphate radicals react with water and form OH· radicals (Eqs. (12)–(15)) [38,39].
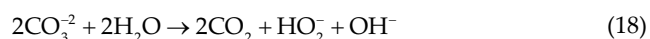
$$S_2O_8^{2-} + hv/us \rightarrow 2SO_4^- \qquad (12)$$

$$SO_4^- + H_2O \rightarrow SO_4^{2-} + OH^\bullet + H^+ \qquad (13)$$

$$SO_4^- + dye \rightarrow SO_4^{2-} + dye + H^+ \qquad (14)$$

$$SO_4^- + dye \rightarrow SO_4^{2-} + CO_2 + H_2O + other\ inorganics \qquad (15)$$

3.6. Effect of scavengers

For environmental samples application, the effect of scavengers was also studied. Anions such as Cl^-, SO_4^{-2}, CO_3^{-2}, PO_4^{3-}, BrO_3^-, HCO_3^- are present in environmental samples; therefore, the effect of these anions was investigated for both dyes. As these anions react with OH· and trap the formation of free oxidizing radicals, it was observed that these anions decrease the efficiency of sonophotocatalytic degradation [39–41]. Chlorides, carbonates, and sulphates were studied as scavengers.

For AR-27 and DV-51 dyes, the effect of chlorides as scavenger was investigated first. Chloride concentration of 0.1 M was studied for degradation at optimized conditions. It was found that it increases the degradation time and decreases the percent removal of AR-27 from 100% degradation in 50–60 min with 81.8% (Fig. 7(a)); in the case of DV-51 it affects the degradation of dye and decreases the removal from 60 min with 100% degradation to 77.7% in 60 min (Fig. 7(b)). The possible reaction that may occur is shown in the following equation [38]:

$$Cl^- + OH^\bullet \rightarrow Cl^\bullet + OH^- \qquad (16)$$

The same concentration (0.1 M) of carbonates was studied on the degradation of both dyes. It was found that in the case of AR-27, 100% degradation in 50 min was declined to 94.6% degradation in 60 min (Fig. 7(a)), and in the case of DV-51, the degradation fell from 100% to 92.9% (Fig. 7(b)). The possible reaction that can occur is given in Eqs. (17)–(19) [38]. The carbonate ions may block the active sites of Cu-Al$_2$O$_3$ photocatalyst, which cause deactivation of the photocatalyst for dye degradation.

$$CO_3^{-2} + OH^\bullet \rightarrow CO_3^- + OH^- \qquad (17)$$

$$2CO_3^{-2} + 2H_2O \rightarrow 2CO_2 + HO_2^- + OH^- \qquad (18)$$

$$OOH^- + OH^\bullet \rightarrow OH^- + OOH \qquad (19)$$

For AR-27 and DV-51, the effect of sulphates (0.1 M) as radical's scavenger was also investigated. It was found that sulphates increase the degradation of AR-27 from 50 min

to 60 min with decrease in degradation from 100% to 93.5% (Fig. 7(a)), and in the case of DV-51 the degradation decreased from 100% to 92.2% in 60 min (Fig. 7(b)). The possible reaction is given in the following equation:

$$SO_4^{-2} + OH^\bullet \rightarrow SO_4^{\bullet-} + OH^- \qquad (20)$$
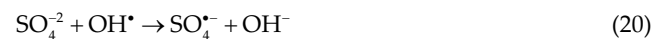
The decrease in the degradation efficiency of AR-29 and DV-51 was observed with all three studied scavengers, which confirms that the dominant controlling mechanism of sonophotocatalytic degradation is the free radical attack.

3.7. The influence of initial dye concentration

Sonophotocatalytically the effect of concentration of dye was studied from 10 to 100 μg/mL. It was found that by applying ultrasonic radiations for 10 μg/mL of AR-27 with 0.02 g of Cu-Al$_2$O$_3$, pH 10, and 8 mmol of H$_2$O$_2$, 100% degradation of AR-27 was achieved in 50 min (Fig. 8). While 10 μg/mL of DV-51 with 0.04 g of Cu-Al$_2$O$_3$, pH 10 and 8 mmol of H$_2$O$_2$, 100% degradation was achieved in 60 min. The rate of degradation decreased with the increase in concentration of AR-27 and DV-51 dyes. Fig. 8 shows that the efficiency of photocatalyst decreased with the increase in initial concentration of AR-27 and DV-51 dyes [42]. AR-27 with 100 μg/mL degraded 82.6% in 60 min, while in the case of DV-51, 100 μg/mL was degraded 43% in 60 min. It demonstrated that with the increase in the initial concentration of dye there may
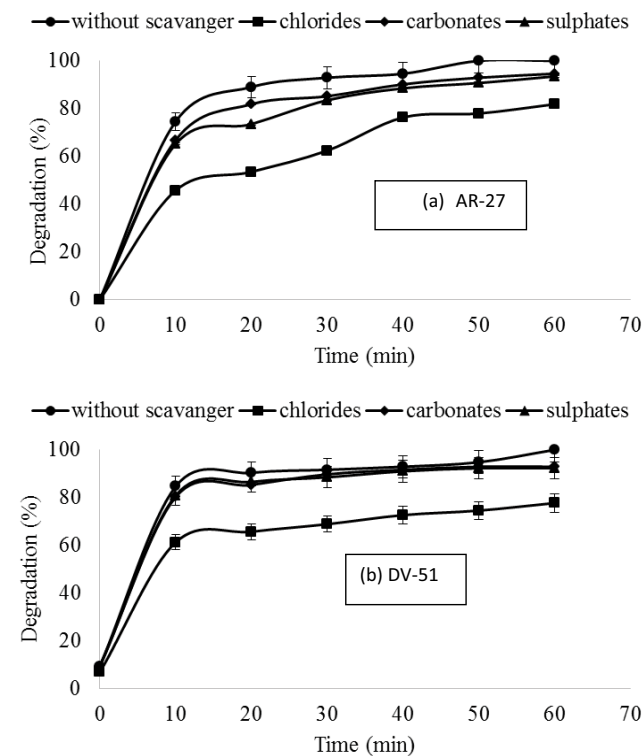

Fig. 7. Effect of scavengers on the degradation of AR-27 and DV-51. Conditions: pH 10, 0.02g Cu-Al$_2$O$_3$, 8 mmol of H$_2$O$_2$ for AR-27, 0.04g and 8 mmol of H$_2$O$_2$ for DV-51, tungsten filament lamp (100W).
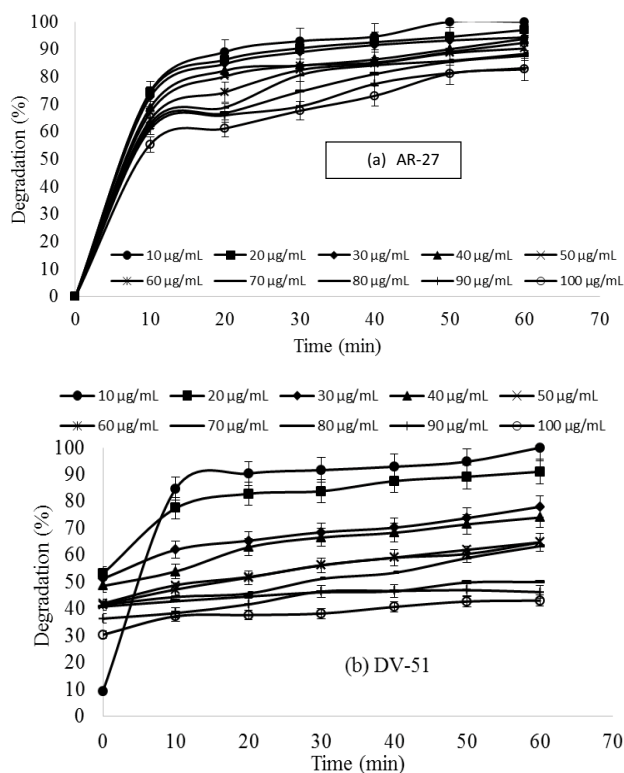
Fig. 8. Effect of dye concentration on degradation of (a) AR-27 and (b) DV-51. Conditions: pH 10, 0.02g Cu-Al$_2$O$_3$, 8 mmol of H$_2$O$_2$ for AR-27, 0.04 g and 8 mmol of H$_2$O$_2$ for DV-51, tungsten filament lamp (100W).

be a decrease in OH·, which is insufficient for the degradation of dye. With the increase in the initial concentration of dye, a decrease in the concentration of OH· radicals occurred; this may be because of an increase in the initial concentration of dye, and because more molecules of dye are adsorbed on the surface of catalyst (Cu-Al$_2$O$_3$). As the intensity of light and catalyst is constant and at that time the light penetration is less because of the intense color of the solution and the path length of the photons entering the solution is decreased, it results in fewer photons reaching the catalyst surface. Hence, the production of OH· radicals is reduced. Therefore, the dye initial concentration also effects the degradation [43].

3.8. Catalyst reusability

In order to investigate the reusability of Cu-Al$_2$O$_3$ after the dye degradation, the solution was filtered and the catalyst was washed with different polar organic solvents (ethanol, methanol, acetone, and acetonitrile) and finally with distilled water. Due to solubility of the adsorbed dye in organic solvents the effect of the solvents used for washing of catalyst was the same (Fig. S3). Therefore, for further washing of the catalyst, ethanol was selected for cost, availability, and safety point of view. Fresh dye solution at optimized conditions of degradation was used after drying of catalyst. The catalyst was run for 5 times, it was found that in case of AR-27 dye it decreases the removal of dye up to 79% and increase the degradation time by using again and

again (Fig. S4). Reusability of catalyst for DV-51 dye was also checked and found that it could be used up to 5 runs and it was observed that at fifth run the DV-51 was degraded 84.6% in 60 min (Fig. S4).

3.9. Sample application

The suggested method was applied to two different samples of dyes. One sample was collected from wastewater of fabric dyeing small scale industry and the second was prepared synthetically. The suggested sonophotocatalytic degradation method was applied at optimized conditions of pH, H$_2$O$_2$, catalyst weight to both synthetic and real samples. It was noted that synthetic dye sample was degraded 93.9% and real sample (industrial sample) was degraded 91.6% in 60 min (Fig. 9).

3.10. Kinetic model

The kinetics study of the sonophotocatalytic degradation of AR-27 and DV-51 dyes was performed and the rate constants determination using pseudo-first-order kinetic model was used. The linear form of pseudo-first-order kinetic equation is as follow:

$$\log\left(q_e - q_t\right) = \log q_e - \frac{K_1 t}{2.303}$$

where, q_e and q_t are the amount (mg g^{-1}) of dye degraded at equilibrium and at any given time (min), respectively. The rate constant is K_1 (min^{-1}). A plot of $\log(q_e - q_t)$ versus time (min) is given in Fig. 10. The rate constant K_1 for AR-27 was found to be 5.82×10^{-2}, and for DV-51 it was found to be 3.84×10^{-2}; the values show that the rate constant of AR-27 is close to the rate constant of DV-51. The R^2 values of AR-27 (0.9297) and DV-51 (0.9614) are also close to each other.

3.11. Mechanism of degradation

The degradation of organic compounds using sonophotocatalytic degradation occurs in different regions of the aqueous solution: (1) bulk solution, (2) interface between the
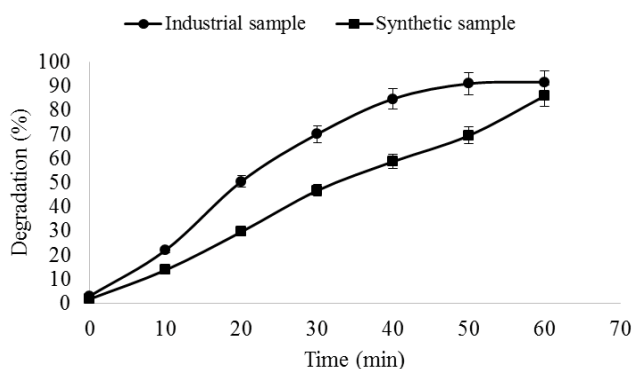

Fig. 9. Proposed degradation method to samples. Conditions: pH 10, 0.02 g Cu-Al$_2$O$_3$, 8 mmol of H$_2$O$_2$, tungsten filament lamp (100 W).
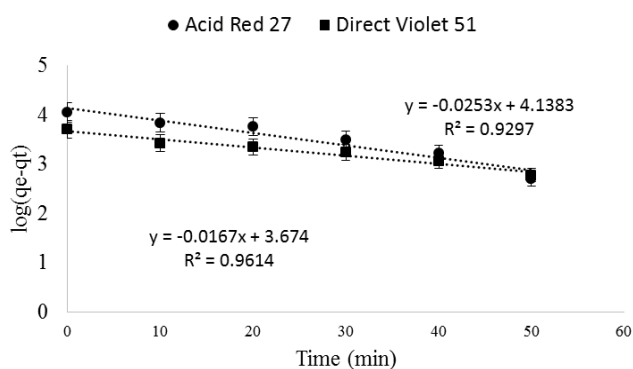
Fig. 10. First order kinetic model to AR-27 and DV-51.

$y = -0.0253x + 4.1383$
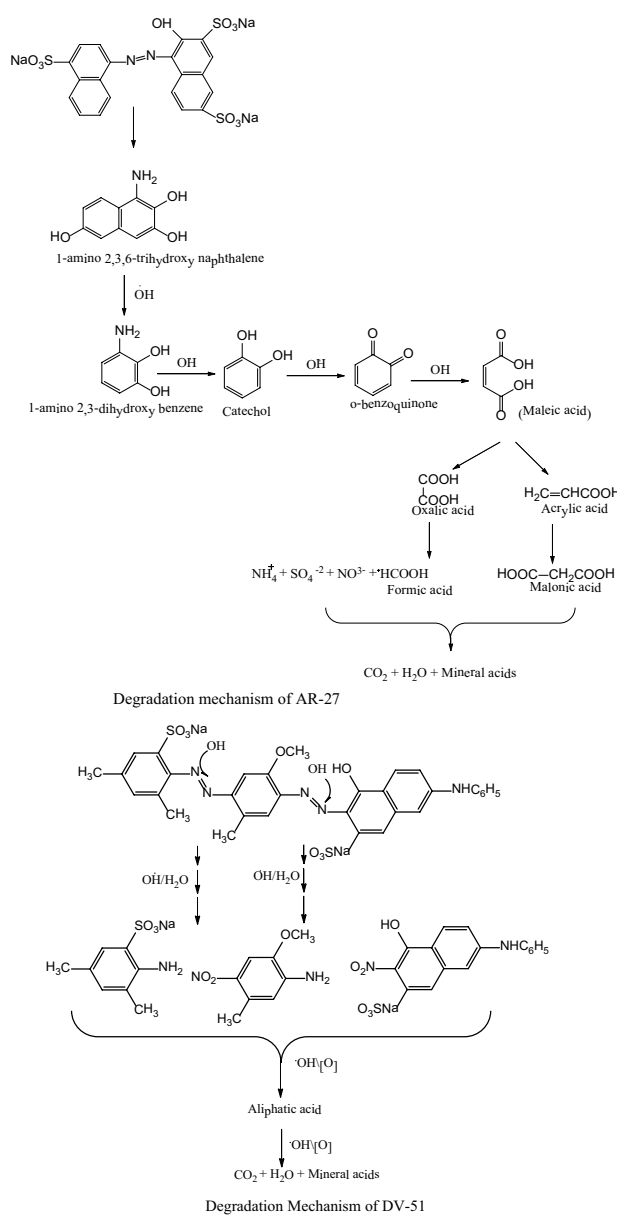$R^2 = 0.9297$

$y = -0.0167x + 3.674$
$R^2 = 0.9614$

Fig. 11. Degradation mechanism of AR 27 and DV-51.

Table 1
Comparison of the proposed degradation method with other degradation methods used for Acid Red-27 and Direct Violet-51

No.	Dye	Degradation Source	Catalyst	Time	% Degradation (%)	References
1.	Acid Red-27	UV (Mercury Lamp) (30 W) 254 nm	Immobilization of ZnO on glass plates	100 min	37.8	[12]
2.	Acid Red-27	UV Lamp (6 W)	TiO_2 UV aqueous suspension	100 min	64	[24]
3.	Acid Red-27	Ultrasonic waves	Zeolite Y encapsulated with Fe-TiO_2	2 h	97.5	[35]
4.	Acid Red-27	Ultrasonic waves	La^{3+} doped TiO_2	90 min	100	[37]
5.	Acid Red-27	Ultrasonic waves	La loaded TiO_2 encapsulated Zeolite Y	120 min	50	[38]
6.	Acid Red-27	Ultrasonic waves	Zeolite Y co-incorporated with Fe and TiO_2	120 min	100	[39]
7.	Acid Red-27	Mercury vapor Lamp (8 W)	ZnO	40 min	84.2	[40]
8.	Acid Red-27	Ultrasonic waves	Fe loaded on encapsulated titanium	120 min	98	[41]
9.	Acid Red-27	Ultrasonic waves	TiO_2–Zeolite	120 min	68	[42]
10.	Direct Violet 51	UV Lamp (350 nm)	TiO_2	60 min	92	[43]
11.	Direct Violet 51	UV Lamp (365 nm)	TiO_2	480 min	82	[44]
12.	Acid Red-27	Ultrasonic waves with Tungsten Lamp (100 W)	Cu-Al_2O_3	50 min	100	Present work
13.	Direct Violet 51	Ultrasonic waves with Tungsten Lamp (100 W)	Cu-Al_2O_3	60 min	100	Present work

bulk solution and cavitation bubbles, (3) interface between the particles of catalyst and cavitation bubbles, and (4) inside the cavitation bubbles. In the cavitation bubble and in the interface of cavitation bubble with bulk solution, there is formation of OH· radical mainly. While in the bulk solution of dye molecules and in the interface of cavitation with photocatalyst OH· radicals, electron (e⁻) transfers directly from the surface of photocatalyst (Cu-Al₂O₃) to the dye molecules as well as direct reaction with holes (h+). The hydrophilic compounds mainly degraded through the OH· radical reaction at the interface of bulk solution and cavitation. The impregnation of copper on Al₂O₃ catalyst enhanced the absorption of photons in the visible region on the surface of photocatalyst, which results in the increased interaction of dye molecules with OH·. The degradation process through OH· was also confirmed by the addition of OH· radical scavengers and observed decrease in degradation efficiency. The degradation mechanism of AR-27 and DV-51 is given in Fig. 11.

3.12. Comparison with other methods of removal

The proposed sonophotocatalytic degradation method for AR-27 and DV-51 using Cu-Al₂O₃ photocatalyst method was compared with other degradation methods using different sources of irradiation, and the photocatalysts in the literature and the comparison data are given in the Table 1. It can be concluded that the proposed sonophotocatalytic degradation method using Cu-Al₂O₃ photocatalyst is superior as compared to other degradation methods.

4. Conclusion

Copper impregnated alumina (Cu-Al₂O₃) photocatalyst was prepared via wet impregnation method to improve the ability of Al₂O₃ to absorb visible light. The photocatalyst was characterized using SEM, EDX, XRD, and UV-visible spectroscopic techniques. The results showed successful impregnation of copper onto Al₂O₃ surface. The degradation of two dyes, AR-27 and DV-51, were investigated in the presence of Cu-Al₂O₃ photocatalyst. The results divulged that there was an increase in degradation using visible irradiation source with ultrasonication. The photocatalyst showed good stability revealed from the reusability performance. It is concluded that Cu-Al₂O₃ acts as a good photocatalyst for the treatment of dyes effluents.

Acknowledgment

References

[1] M. Nasirian, M. Mehvar, Photocatalytic degradation of aqueous methyl orange using nitrogen doped TiO₂ photocatalysts prepared by novel method of ultraviolet-assisted thermal synthesis, J. Environ. Sci., 66 (2018) 81–93.

[2] M. Nasirian, M. Mehvar, Modification of TiO₂ to enhance photocatalytic degradation of organics in aqueous solutions, J. Environ. Chem. Eng., 4 (2016) 4072–4082.

[3] W.T. Yein, Q. Wang, X. Feng, Y. Li, X. Wu, Enhancement of photocatalytic performance in sonochemical synthesized ZnO–rGO nanocomposites owing to effective interfacial interaction, Environ. Chem Lett., 16 (2018) 251–264.

[4] J. Shah, M.R. Jan, F. Khitab, Sonophotocatalytic degradation of textile dyes over Cu impregnated ZnO catalyst in aqueous solution, Process Saf. Environ. Prot., 116 (2018) 149–158.

[5] R. Saravanan, S. Karthikeyan, V.K. Gupta, G. Sekaran, V. Narayanan, A. Stephen, Enhanced photocatalytic activity of ZnO/CuO nanocomposite for the degradation of textile dye on visible light illumination, Mater. Sci. Eng. C., 33 (2013) 91–98.

[6] M. Yazdanmehr, S.J. Asadabadi, A. Nourmohammadi, M. Ghasemzadeh, M. Rezvanian, Electronic Structure and band gap of γ-Al₂O₃ compound using mBj exchange potential, Nanoscale Res. Lett., 7 (2012) 488–498.

[7] H.P. Pinto, R.M. Nieminea, S.D. Elliozz, Ab initio Study of; γ-Al₂O₃ surfaces, Phys. Review: B, 70 (2004) 125402.

[8] E.O. Filatova, A.S. Konashak, Interpretation of the changing of the band gap of Al₂O₃ depending on its crystalline form; connection with different local symmetries, J. Phy. Chem. C., 119 (2015) 20755–20761.

[9] H.A.P. Alibad, S.R. Ghorbani, Structural and spin polarization effects of Cr, Fe and Ti elements on electronic properties of α-Al₂O₃ by first principle calculations, J. Moder. Physic., 2 (2011) 158–161.

[10] Z. Boutamine, S. Merouani, O. Hamdaoui, Sonochemical degradation of Basic Red 29 in aqueous media, Turkish J. Chem., 41 (2017) 99–115.

[11] C.I. Pearce, J.R. Lloyd, J.T. Guthrie, The removal of colour from textile wastewater using whole bacterial cells : A review, Dyes Pig., 58 (2003) 179–196.

[12] M.A. Behnajady, N. Modirshahla, N. Daneshvar, M. Rabbani, Photocatalytic degradation of C.I. Acid Red 27 by immobilized ZnO on glass plates in continuous-mode, J. Hazard. Mater., 140 (2007) 257–263.

[13] W. Baran, A. Makowski, W. Wardas, The effect of UV radiation absorption of cationic and anionic dye solutions on their photocatalytic degradation in the presence TiO₂, Dyes Pig., 76 (2008) 226–230.

[14] J. Shah, M.R. Jan, S. Jamil, A.U. Haq, Magnetic particles precipitated onto wheat husk for removal of methyl blue from aqueous solution, Toxicolog. Environ. Chem., 96 (2014) 218–226.

[15] G. Sharma, M. Naushad, A. Kumar, S. Rana, S. Sharma, A. Bhatnagar, F.J. Stadler, A.A. Ghfar, M.R. Khan, Efficient removal of coomassie brilliant blue R-250 dye using starch/poly (alginic acid-cl-acrylamide) nanohydrogel, Pro. Saf. Environ. Protec., 109 (2017) 301–310.

[16] A. Pirkarami, M.E. Olya, Removal of dye from industrial wastewater with an emphasis on improving economic efficiency and degradation mechanism, J. Saudi Chem. Soc., 21 (2017) S179–S186.

[17] B.S. Zeb, Q. Mahmood, A. Pervez, Characteristics and performance of anaerobic wastewater treatment (a review), J. Chem. Soc. Pak., 35 (2013) 217–232.

[18] T. Robinson, G. McMullan, R. Marchant, P. Nigam, Remediation of dyes in textile effluent: A critical review on current treatment technologies with a proposed alternative, Bioresour. Technol., 77 (2001) 247–255.

[19] N. Daneshvar, M. Rabbani, N. Modirshahla, M.A. Behnajady, Critical effect of hydrogen peroxide concentration in photochemical oxidative degradation of C.I. Acid Red 27 (AR27), Chemosphere, 56 (2004) 895–900.

[20] N. Daneshvar, D. Salari, A.R. Khataee, Photocatalytic degradation of azo dye acid red 14 in water on ZnO as an alternative catalyst to TiO₂, J. Photochem. Photobiol. A: Chem., 162 (2004) 317–322.

[21] N. Daneshvar, D. Salari, A.R. Khataee, Photocatalytic degradation of azo dye acid red 14 in water: investigation of the effect of operational parameters, J. Photochem. Photobiol. A: Chem., 157 (2003) 111–116.

[22] M. Pérez-Urquiza, J.L. Beltran, Determination of dyes in foodstuffs by capillary zone electrophoresis, J. Chromatogr. A, 898 (2000) 271–275.

[23] M.S. Larrechi, M.P. Callao, An analytical overview of processes for removing organic dyes from wastewater effluents, Trend. Anal. Chem., 29 (2010) 1202–1212.

[24] N. Daneshvar, M. Rabbani, N. Modirshahla, M.A. Behnajady, Kinetic modeling of photocatalytic degradation of Acid Red 27 in UV/TiO$_2$ process, J. Photochem. Photobiol. A: Chem., 168 (2004) 39–45.

[25] Adnan, J. Shah, M.R. Jan, Polystyrene degradation studies using Cu supported catalysts, J. Anal. Appl. Pyrol., 109 (2014) 196–204.

[26] S. Brunauer, P.H. Emmett, E. Teller, Adsorption of gases in multimolecular layers, J. Amer. Chem. Soc., 60 (1938) 309–319.

[27] N. Daneshvar, M. Rabbani, N. Modirshahla, Toxic/hazardous substances and environmental engineering photooxidative degradation of Acid Red 27 (AR 27): Modeling of reaction kinetic and influence of operational parameters, J. Environ. Sci. Health, 39 (2012) 2319–2332.

[28] C. Turchi, Photocatalytic degradation of organic water contaminants: Mechanisms involving hydroxyl radical attack, J. Catal., 122 (1990) 178–192.

[29] Y. Huang, G. Wang, H. Zhang, G. Li, D. Fang, Y. Song, Hydrothermal-precipitation preparation of CdS@(Er^{3+}:Y$_3$Al$_5$O$_{12}$/ZrO$_2$) coated composite and sonocatalytic degradation of caffeine, Ultrason. Sonochem., 37 (2017) 222–234.

[30] A. Khataee, S. Saadi, B. Vahid, S.W. Joo, B.K. Min, Sonocatalytic degradation of Acid Blue 92 using sonochemically prepared samarium doped zinc oxide nanostructures, Ultrason. Sonochem., 29 (2016) 27–38.

[31] A. Khataee, A. Karimi, S. Arefi-Oskoui, R.D.C. Soltani, Y. Hanifehpour, B. Soltani, S.W. Joo, Sonochemical synthesis of Pr-doped ZnO nanoparticles for sonocatalytic degradation of Acid Red 17, Ultrason. Sonochem., 22 (2015) 371–381.

[32] M. Rauf, S.S. Ashraf, Fundamental principles and application of heterogeneous photocatalytic degradation of dyes in solution, Chem. Eng. J., 15 (2009) 10–18.

[33] M. Behnajady, N. Modirshahla, M. Shokri, Photodestruction of Acid Orange 7 (AO7) in aqueous solutions by UV/$_{H2O2}$: Influence of operational parameters, Chemosphere, 55 (2004) 129–134.

[34] V.K. Mahajan, S.P. Patil, S.H. Sonawane, G.H. Sonawane, Ultrasonic, photocatalytic and sonophotocatalytic degradation of Basic Red-2 by using Nb$_2$O$_5$ nano catalyst, AIMS Biophysics, 3 (2016) 415–430.

[35] A.H. Alwash, A.Z. Abdullah, N. Ismail, Zeolite Y encapsulated with Fe-TiO$_2$ for ultrasound-assisted degradation of amaranth dye in water, J. Hazard. Mater., 233–234 (2012) 184–193.

[36] V.K. Gupta, R. Jain, A. Mittal, T.A. Saleh, A. Nayak, S. Agarwal, S. Sikarwar, Photo-catalytic degradation of toxic dye amaranth on TiO$_2$/UV in aqueous suspensions, Mater. Sci. Eng. C, 32 (2012) 12–17.

[37] L. Song, C. Chen, S. Zhang, Q. Wei, Sonocatalytic degradation of amaranth catalyzed by La^{3+} doped TiO$_2$ under ultrasonic irradiation, Ultrason. Sonochem., 18 (2011) 1057–1061.

[38] A.H. Alwash, A.Z. Abdullah, N.L. Ismail, La loaded TiO$_2$ encapsulated zeolite Y catalysts: Investigating the characterization and decolorization process of amaranth dye, J. Eng., 2013 (2013) 1–10.

[39] A.H. Alwash, A.Z. Abdullah, N. Ismail, Elucidation of reaction behaviors in sonocatalytic decolorization of amaranth dye in water using zeolite Y co-incorporated with Fe and TiO$_2$, Adv. Chem. Eng. Sci., 2013 (2013) 113–122.

[40] M. Shanthi, V. Kuzhalosai, Photocatalytic degradation of an azo dye, Acid Red 27, in aqueous solution using nano ZnO, Indian J. Chem., 51 (2012) 428–434.

[41] A.H. Alwash, A.Z. Abdullah, N. Ismail, Investigation on the catalytic behavior of Fe loaded on encapsulated titanium for sonocatalytic degradation of amaranth: Characterization and reusability Study, Modern Res. Catal., 2013 (2013) 100–109.

[42] A.H. Alwash, A.Z. Abdullah, N. Ismail, TiO$_2$-zeolite Y catalyst prepared using impregnation and ion-exchange method for sonocatalytic degradation of amaranth dye in aqueous solution, Int. J. Chem. Mole. Eng., 7 (2013) 375–383.

[43] W.Z. Tang, Z. Zhang, H. An, M.O. Quintana, D.F. Torres, TiO$_2$/UV photodegradation of azo dyes in aqueous solutions, Environm. Technol., 18 (1997) 1–12.

[44] R. Byberg, J. Cobb, L.D. Martin, R.W. Thompson, T.A. Camesano, O. Zahraa, M.N. Pons, Comparison of photocatalytic degradation of dyes in relation to their structure. Environm, Sci. Pollut. Res., 20 (2013) 3570–3581.

Supplementary Information

Table S1.1
X-Ray Diffraction data for Al$_2$O$_3$

2θ	Height from base	Width (at half height)	Area	Thickness (nm)	d Bragg's law
13.2	480.3	0.091696894	2686.8	1.552098783	1.340389272
16.6	1227.8	0.059042747	4421.8	2.401167172	1.067224759
23	66.17	0.003298575	13.35	42.56262773	0.772744538
25.5	787.32	0.003490556	168.2	40.03360733	0.698061889
31.6	95.62	0.003438197	20.07	40.09638822	0.565815661
33.9	29.25	0.00335966	5.99	40.79241646	0.528441942
35.1	1152.7	0.003642395	256.1	37.50383007	0.510915444
37.7	420.36	0.003818668	97.90	35.50675825	0.476831773
38.9	96.87	0.00345565	20.45	39.09434366	0.462665807
43.3	1253.6	0.003874517	297.49	34.36958331	0.417580314
44.6	26.30	0.004183431	6.71	31.6862762	0.406002928
47.1	41.79	0.004014139	10.26	32.71931961	0.385585264
51.5	74.79	0.003590036	16.37	35.94552289	0.354613685
52.5	433.47	0.004309091	113.93	29.82013709	0.34832503
57.5	900.96	0.004670363	256.72	26.8954419	0.320298863
61.2	43.86	0.011117419	29.84	11.09263259	0.302647483
66.5	248.71	0.005549983	84.45	21.58885789	0.280981076
68.2	407.42	0.005328333	132.4	22.26575087	0.274793576
77	89.25	0.009578084	52.14	11.70669006	0.247479865

Table S1.2
X-Ray Diffraction data for Cu-Al$_2$O$_3$

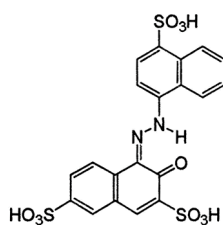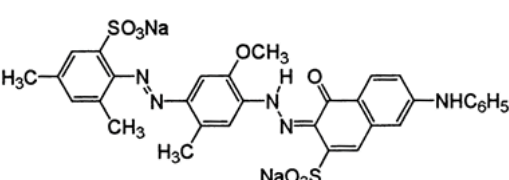| 2θ	Height from base	Width (at half height)	Area	Thickness (nm)	D Bragg's law
13.7	456.08	0.196518278	5468.89	0.723848375	1.291690635
16.4	526.03	0.051991825	1668.38	2.727493901	1.080149087
22.9	41.76	0.006998564	17.83	20.06424371	0.776073636
25.5	608.98	0.003577819	132.9	39.05717789	0.698061889
26.4	40.64	0.003804706	9.47	36.66167978	0.674665539
29.3	540.2	0.003403292	112.5	40.72951245	0.60914223
31.7	78.66	0.007941014	38.17	17.35612092	0.5640763
33.9	27.63	0.002268861	3.84	60.40415514	0.528441942
35.1	903.59	0.003804706	210.50	35.90389604	0.510915444
37.7	348.54	0.003368386	73.13	40.25325754	0.476831773
38.9	216.59	0.003682536	48.73	36.68568742	0.462665807
43.3	973.47	0.003857064	229.04	34.52510178	0.417580314
44.6	41	0.004433006	11.08	29.9023638	0.406002928
47.8	54.51	0.003682536	12.28	35.56999197	0.380262807
51.4	60.15	0.003804706	14.01	33.93166675	0.35525656
52.5	344.21	0.0043981	92.68	29.21663432	0.34832503
57.4	691.07	0.004502817	190.31	27.90954664	0.320809286
59.3	21.61	0.003298575	4.36	37.74770153	0.31142104
61.1	45.55	0.013089583	36.39	9.426200994	0.303094847
66.5	212.39	0.005427814	70.41	22.07478074	0.280981076
68.1	353.22	0.005166022	111.40	22.97887583	0.275148328
76.9	64.12	0.010977797	42.99	10.22112622	0.247751768
78.1	52.71	0.005846681	18.80	19.0306972	0.244540037

Table S1.3
X-Ray Diffraction data for reused Cu-Al$_2$O$_3$

2θ	Height from base	Width (at half height)	Area	Thickness (nm)	D Bragg's law
12.7	30.81	0.012269303	23.06	11.60564164	1.392931352
14.7	59.32	0.009948083	36.05	14.28364678	1.204254956
16.7	26.99	0.006474981	10.66	21.89248348	1.06087909
19.7	69.12	0.036650833	154.60	3.851487563	0.900573279
21.7	249.93	0.089916711	1370.81	1.564903841	0.818432625
30	55	0.004537722	15.58	30.49778761	0.595243829
32.5	613.34	0.004275931	160.42	32.16812647	0.550551992
38.6	76.81	0.004328289	20.34	31.24116697	0.466123031
40.9	30.87	0.003979233	7.52	33.73595447	0.440941116
42.1	1019.49	0.004415553	274.69	30.28198659	0.428919367
44.7	371.66	0.004241025	96.53	31.24477084	0.40514103
45.9	91.55	0.005061306	28.33	26.06681336	0.395099663
48.6	14.47	0.004782061	4.23	27.30608781	0.374373979
50.3	1084.36	0.004415553	292.69	29.3712778	0.362503641
54.1	8.45	0.004380647	31.56	29.12821974	0.338766674
55.7	11.57	0.006422622	4.54	19.72377504	0.329781458
58.4	74.98	0.003665083	16.82	34.12375678	0.31578783
59.5	423.06	0.00471225	121.79	26.3971009	0.310469577
64.5	848.54	0.004886778	253.12	24.79557262	0.288710387
66.4	19.13	0.011169778	13.04	10.73309664	0.28135568
68.2	57.07	0.010332044	36	11.48265835	0.274793576
73.5	265.51	0.005584889	90.65	20.5552741	0.25748549
75.2	392.27	0.005584889	133.80	20.32532415	0.252497079

Table S1.4
X-Ray Diffraction data after catalyst poisoning Cu-Al$_2$O$_3$

2θ	Height from base	Width (at half height)	Area	Thickness (nm)	D Bragg's law
11.6	33.34	0.018499944	37.98	7.704816204	1.524502009
13.8	33.88	0.011850436	24.50	12.00246718	1.282375358
18	28.02	0.017190986	29.39	8.23153866	0.984824579
18.9	22.19	0.009180161	12.44	15.39492435	0.938324266
20.8	13.16	0.006963658	5.59	20.23626981	0.853430219
22.6	147.5	0.064749806	582.53	2.169811382	0.786238919
29	29.24	0.005166022	9.23	26.8502124	0.615306509
31.5	333.45	0.005445267	111.06	25.32351258	0.567566215
37.6	46.64	0.005183475	14.78	26.16562351	0.478053922
39.9	25.04	0.004223572	6.47	31.8864985	0.451525114
41.1	610.56	0.004904231	182.94	27.35508992	0.438887548
43.7	202.48	0.004956589	61.33	26.82897778	0.413942634
44.9	61.73	0.006317906	23.79	20.95861821	0.403429085
49.3	706.80	0.004782061	206.26	27.23026895	0.369383433
53.1	26.32	0.004485364	7.21	28.57385701	0.344670207
58.5	256.27	0.005061306	79.21	24.6982464	0.315295629
63.5	566.19	0.0050264	174.15	24.23861295	0.292770795
67.2	29.91	0.010873081	19.84	10.9753376	0.278392416
72.5	162.24	0.00534055	52.86	21.63495831	0.260540177
74.2	253.31	0.005864133	90.71	19.4867941	0.255400945

Table S2
Characteristics of Acid Red 27 and Direct Violet 51

S.N.	Basic dyes	Other names	Structure	Molecular formula	λ_{max}	C.I.
1.	Acid Red 27	Amaranth		$C_{20}H_{11}N_2Na_3O_{10}S_3$	521 nm	16185
2.	Direct Violet 51	Violet 2B		$C_{32}H_{27}N_5Na_2O_8S_2$	550 nm	27905
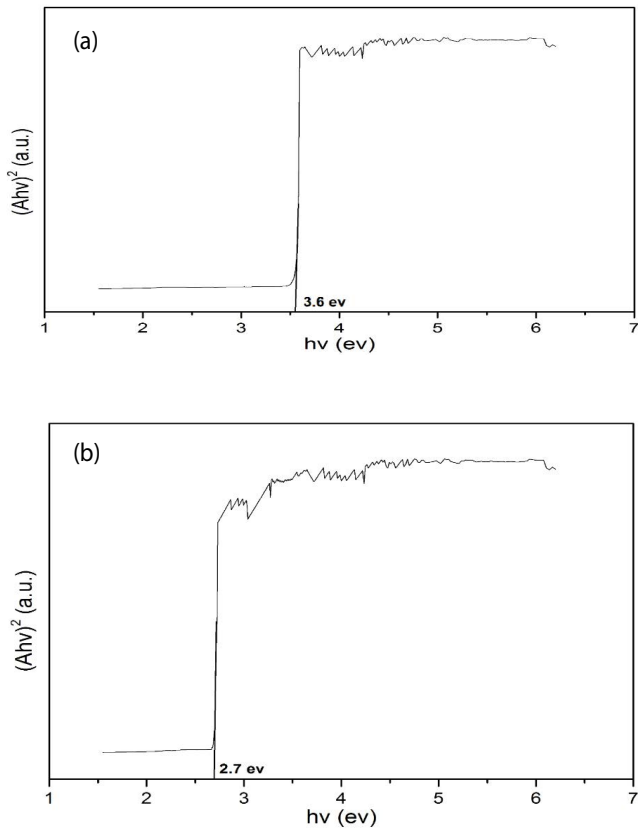
Fig. S1. (a) Tauc plot for Al_2O_3, (b) Tauc plot for $Cu-Al_2O_3$.
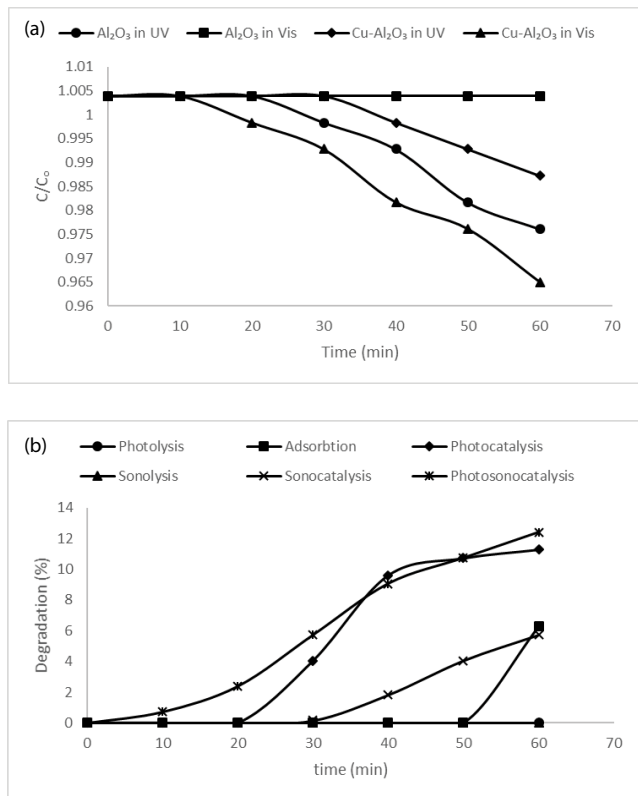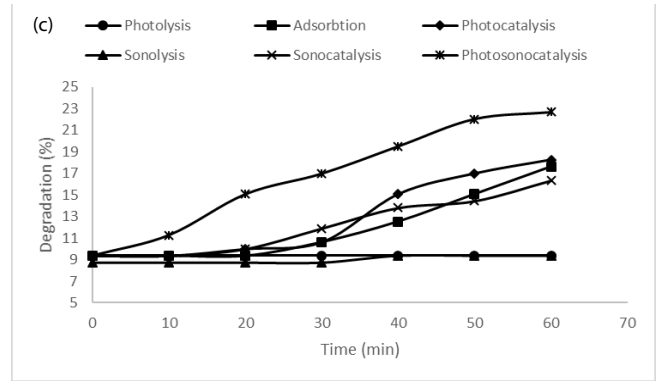

Fig. S2. (a) Degradation of Al_2O_3 and $Cu-Al_2O_3$ in UV and Visible region, (b) Degradation of AR 27 under different conditions, (c) Degradation of DV 51 under different conditions.
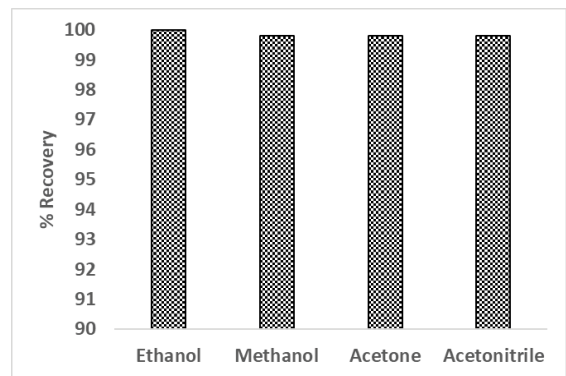
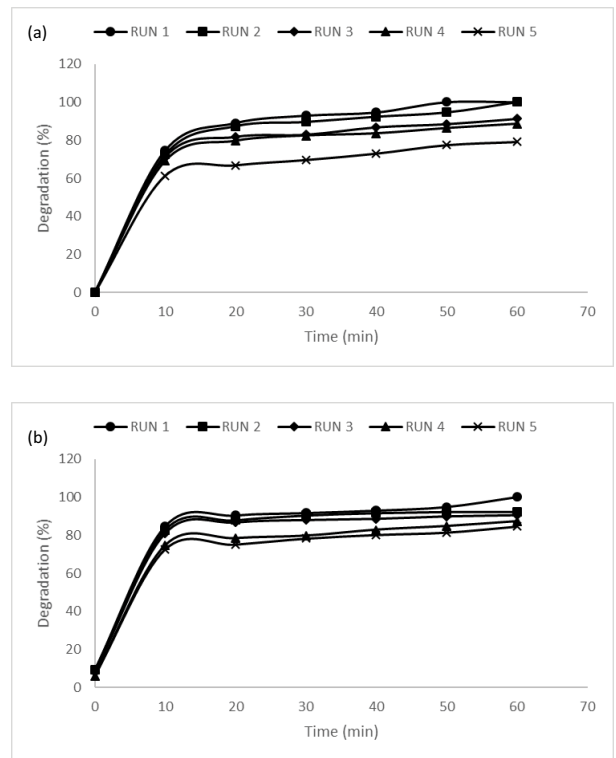

Fig. S3. Desorption of dye with different solvents.

Fig. S2. *(Continued).*

Fig. S4. Reusability of $Cu-Al_2O_3$ using (a) AR-27 and (b) DV 51 dyes.